Deep-Sea Research, Vol. 38, Suppl. 1, pp. S21–S43, 1991.
Printed in Great Britain.

0198–0149/91 $3.00 + 0.00

Estimates of Kuroshio transport using an inverse technique

FREDERICK M. BINGHAM* and LYNNE D. TALLEY

(*Received* 2 *December* 1989; *in revised form* 11 *January* 1990; *accepted* 5 *February* 1990)

Abstract—Two CTD/hydrographic sections across the Kuroshio were combined using an inverse technique to estimate the absolute transport. The hydrographic data were obtained as part of a transpacific section across 24°N in 1985. The inverse technique treats the two sections as ends of a channel and conserves mass flowing into and out of the channel as a whole and within certain discrete layers. The strong topographic constraints imposed by the region of the East China Sea resulted in transport estimates independent of the initial reference level for the geostrophic calculation.

The calculated transports were 26.6 Sv northwest of Okinawa and 21.9 Sv across the Tokara Straits. The accuracy of the estimate was approximately 3.3 Sv for the Okinawa section and 5.1 Sv for the Tokara Straits section. The principal errors in the calculation came from lack of knowledge of the flow in the shallow areas of both sections, inadequate sampling of the rapidly varying topography, an estimate of 5 Sv transport in the Tsushima Current and Osumi branch of the Kuroshio and uncertainty over the relative weighting given in the inverse solutions to the different sections.

A set of acoustic Doppler current profiler (ADCP) data taken simultaneously was combined with the inverse model. Because initial mass imbalances were smaller, the combined model gave a better estimate of transport than that of the model using the CTD data alone. Two different methods of using the ADCP data in the inverse model were compared. It was found to be preferable to use the ADCP data as an initial reference for the geostrophic velocities, rather than as a set of separate constraints.

1. INTRODUCTION

THE transport of the Kuroshio through the East China Sea has been estimated many times from hydrographic sections using standard reference level calculations (e.g. NITANI, 1972; GUAN, 1983). In contrast, the analogous current in the North Atlantic, the Florida Current through the Florida Straits, has been measured directly many times and its transport may be one of the best-known oceanic measurements. In lieu of a direct estimate, the inverse technique used in the present study and in a recent study of North Pacific large-scale circulation by ROEMMICH and MCCALLISTER (1989) is probably the most robust method for calculating geostrophic transports. Accurate knowledge of Kuroshio transport is important for fresh water and heat balances in the North Pacific. There is also observational evidence that the Kuroshio mass transport in the East China Sea is related to the status of the meander of the Kuroshio south of Honshu (GUAN, 1983).

*Scripps Institution of Oceanography, La Jolla, CA 92093, U.S.A.

Corresponding Author Address:
Frederick Bingham
University of Hawaii at Manoa, JIMAR
1000 Pope Road
Honolulu, HI 96822

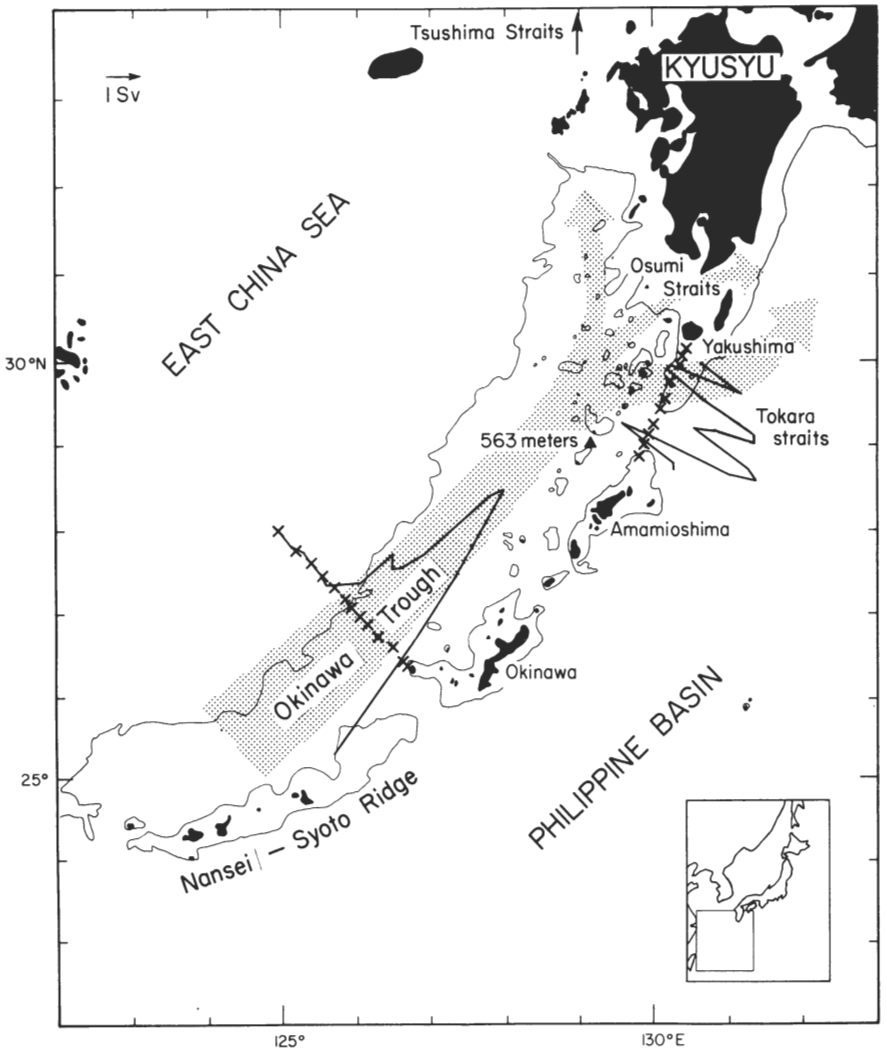

Fig. 1. The bathymetry of the East China Sea. Land areas are darkened. Contours drawn represent the 500 m isobath. The CTD stations on south and north sections are indicated by the Xs. The large arrows schematically show the locations of the Kuroshio and the Tsushima and Osumi branches (following NITANI, 1972). The deepest passage between the north and south sections is indicated just west of the north section and marked by its depth, 563 m (MAEDA, personal communication). Curves associated with sections are vertically integrated transport between grid pairs obtained from the standard model. Arrow in upper left corner shows 1 Sv. The bathymetry in this figure is taken from the 'Bathymetric Chart of the Adjacent Seas of Nippon, #6302', published by the Japanese Maritime Safety Agency in July 1966.

A comprehensive study of the Kuroshio in the East China Sea was made by NITANI (1972), who computed time series of volume transport, referenced to 1200 db, measuring the Kuroshio in three places and various other counter- and parallel currents. In his schematic diagram (his Fig. 28) on which Fig. 1 is based, volume transports of all currents in the East China Sea are approximately balanced. The actual transports varied considerably from year to year, with the sections northwest of Okinawa and southeast of Yakushima having variations 180° out of phase with each other. Nitani showed that the dependence of his computation of geostrophic transport on the reference level becomes stronger farther to the northeast along the path of the Kuroshio. Northwest of Okinawa, in

the area most relevant to the present study, he calculated a mean geostrophic transport of about 30 Sv (1 Sv = 10^6 m^3 s^{-1}) with a spread of ±5–10 Sv.

KONAGA *et al.* (1980) and GUAN (1983), using the same measurements, studied transport variations relative to 700 db through the section G-PN, which crosses the East China Sea northwest of Okinawa and corresponds closely to the southern section used in this study (Fig. 1). The transports were calculated using 23 years of data comprising 71 crossings of the Kuroshio. The calculated mean transport was 21.3 Sv, the standard deviation was 5.4 Sv, the minimum transport was 5 Sv, and the maximum was 35 Sv. The computed transport was highly variable, sometimes changing by as much as 50% in 2 months.

Most previous estimates of Kuroshio transport have been based on an arbitrarily chosen reference level-of-no-motion. Often there has been no physical reasoning stated for choosing the given reference level. NITANI (1972) indicated that without direct measurement of the velocity, inferring the correct reference level is difficult. TAKEMATSU *et al.* (1986) used a number of current meter moorings in the Tokara Straits to infer a reference level in order to place a bound on the maximum Kuroshio transport at that location. The moorings were not spread evenly across the Straits but were bunched together in two separate locations. The reference level found was about 600 m, although the moorings were just offshore of where the Kuroshio flows over a sill of 400 m or less; no moorings were located near the deeper part of the Straits. Mean velocity profiles from two moorings were integrated to produce transport per unit width which was then linearly interpolated across the strait to estimate a net transport of 22 Sv; however, they considered it only a rough guess.

Besides the above-mentioned estimate, direct measurements of transport have not been made for the Kuroshio as they have been for the Florida Current (NIILER and RICHARDSON, 1973), although a program for direct measurement in the Kuroshio is currently in progress. WORTHINGTON and KAWAI (1972) compared a section across the Kuroshio in the East China Sea to one across the Florida Straits and found them to be similar in many respects, having similar temperature and salinity structures and playing analogous roles in their respective ocean's general circulation. NIILER and RICHARDSON's (1973) measurements in the Florida Straits showed that the Florida Current varies greatly in transport, with variations of as much as 6–8 Sv over the course of a few days. The Florida Current has a seasonal cycle, but variations of transport within a given season can be just as large as the seasonal cycle.

The purpose of this study is to estimate the Kuroshio transport in the East China Sea and Tokara Straits using an inverse technique which avoids having to choose an arbitrary level-of-no-motion. It combines two CTD/hydrographic sections using the knowledge that mass is conserved and that water does not flow through the bottom. The technique used in this investigation is that of WUNSCH (1978) and ROEMMICH (1979). ROEMMICH and MCCALLISTER (1989) used a similar method to estimate the transport through a section northwest of Okinawa, one of the sections used here. Although subject to errors, it is believed the estimates made here are more accurate than previous ones. In addition, the estimated absolute velocity field reveals the presence of counter-currents flanking the Kuroshio in the East China Sea.

JOYCE *et al.* (1986) applied this method to the computation of transport of the Gulf Stream, using hydrographic data with simultaneous acoustic Doppler current profiler (ADCP) data. ADCP measurements were made at the same time as the CTD sections studied in this paper. An inversion was done using these ADCP data as an initial

geostrophic reference, but the results were not found to differ significantly from using an arbitrary initial level-of-no-motion. Finally, ADCP and hydrographic data were inverted simultaneously to study the effects of variations in weighting on the outcome of the inversion; the results were sensitive to the relative weighting of the two types of data.

2. SECTIONS

Two sections were used (Fig. 1); the south section extends northwest from Okinawa across the Okinawa trough and onto the shallow continental shelf. At its deepest it is almost 2000 m, decreasing to less than 100 m on the shelf. The north section extends northeastward from near Amamioshima to Yakushima crossing the Tokara Straits and a submarine canyon. Its greatest depth is about 1400 m.

The mean path of the Kuroshio as determined by NITANI (1972) flows through the passage east of Taiwan, passes along the edge of the continental shelf and exits the East China Sea just south of Yakushima (Fig. 1). The Osumi Current flows through the Osumi Straits between Yakushima and Kyusyu, and the Tsushima Current flows into the Japan Sea between Japan and Korea. The Nansei–Syoto Ridge and the Ryukyu Islands act as an effective barrier to exchanges of water from the East China Sea to the Philippine Basin.

The south section was occupied on 31 May and 1 June 1985, and the north section on 2 and 3 June 1985. Both sections were collected as part of a transpacific hydrographic section across approximately 24°N in the North Pacific (henceforth referred to as TPS24). The data were collected using a CTD and rosette sampler. Data from this section and other recent sections have been used in a study of North Pacific circulation by ROEMMICH and MCCALLISTER (1989) and a computation of meridional heat flux by BRYDEN *et al.* (1991). Potential density, potential temperature and specific volume anomaly were computed from the 2 db CTD pressure, temperature and salinity measurements. The data were then smoothed to 10 db intervals using a Gaussian filter with a half-width of 10 db.

The 10 db smoothed data were objectively mapped onto a regular grid with a spacing of 10 km in the horizontal and 10 db in the vertical. The objective mapping procedure used was similar to that of ROEMMICH (1983), with a large-scale field chosen to represent features the size of the section and a small-scale field to represent features on the scale of one station spacing. Specifically, the large-scale field had a horizontal covariance of 20 station spacings or about 300 km and a vertical covariance of 1000 m. The small-scale field had a horizontal covariance of two station spacings and a vertical covariance of 20 m. The resulting fields looked smooth and reasonable. Little difference was found between shear computed from the objectively mapped data and from the smoothed 10 db station data.

Properties

The objectively mapped sections of salinity and potential density in both sections show the signature of the salinity maximum water formed by strong evaporation at the sea surface in the center of the subtropical gyre (Figs 2 and 3). On the inshore side of each section at the surface there is water of low salinity associated with river inflow into the Yellow Sea (NITANI, 1972). The salinity minimum of the North Pacific Intermediate Water is present at greater depths.

In the part of the water column where the salinity minimum is seen, where the temperature is between 4 and 13°C, the waters in both sections are more saline than the

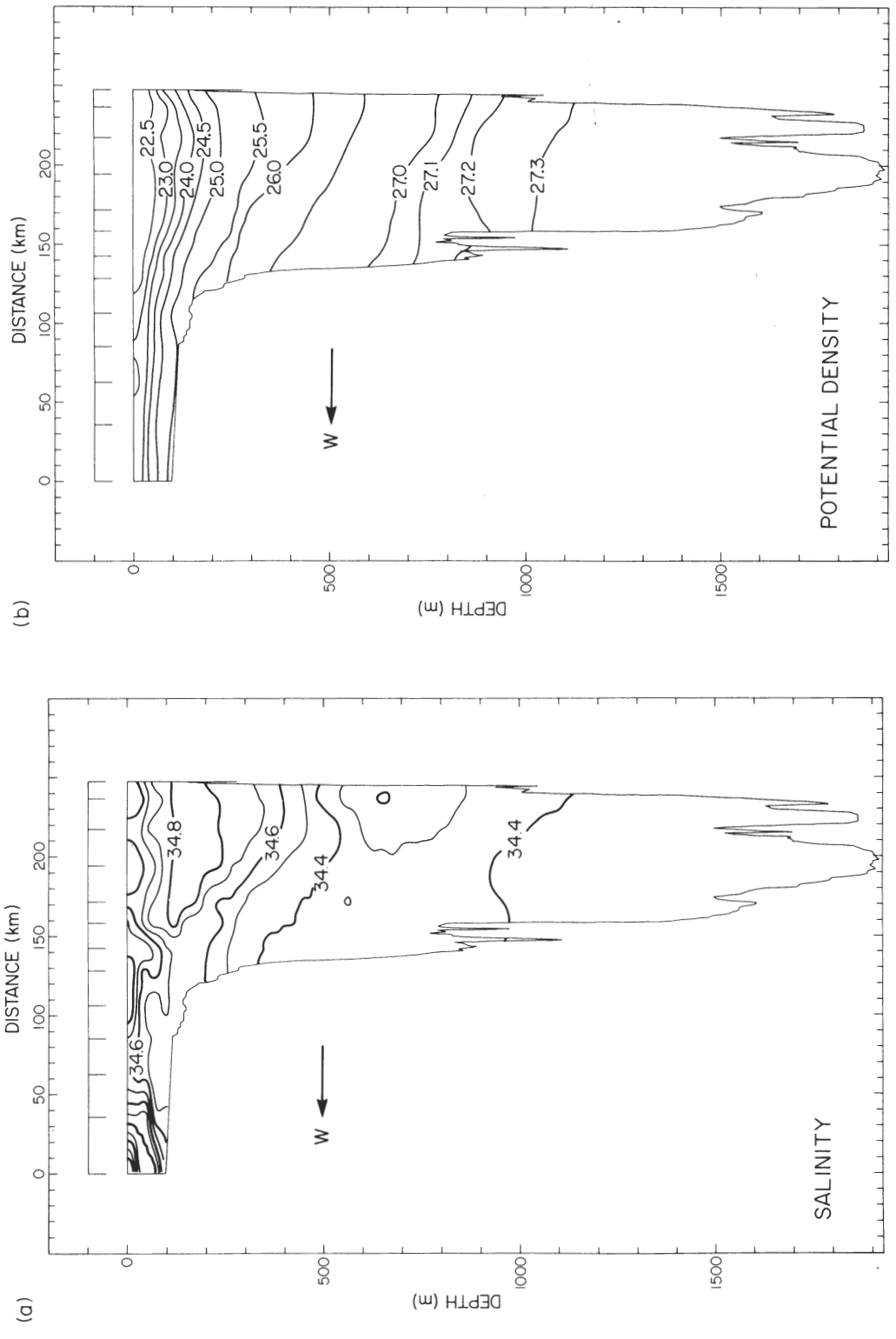

Fig. 2. Properties on the south section. 0 km is on the shelf of the East China Sea. Station locations are indicated above the section. 247 km is next to the Nansei–Syoto Ridge, on the southeast end of the section. (a) Salinity (‰). (b) σ_θ (kg m^{-3}).

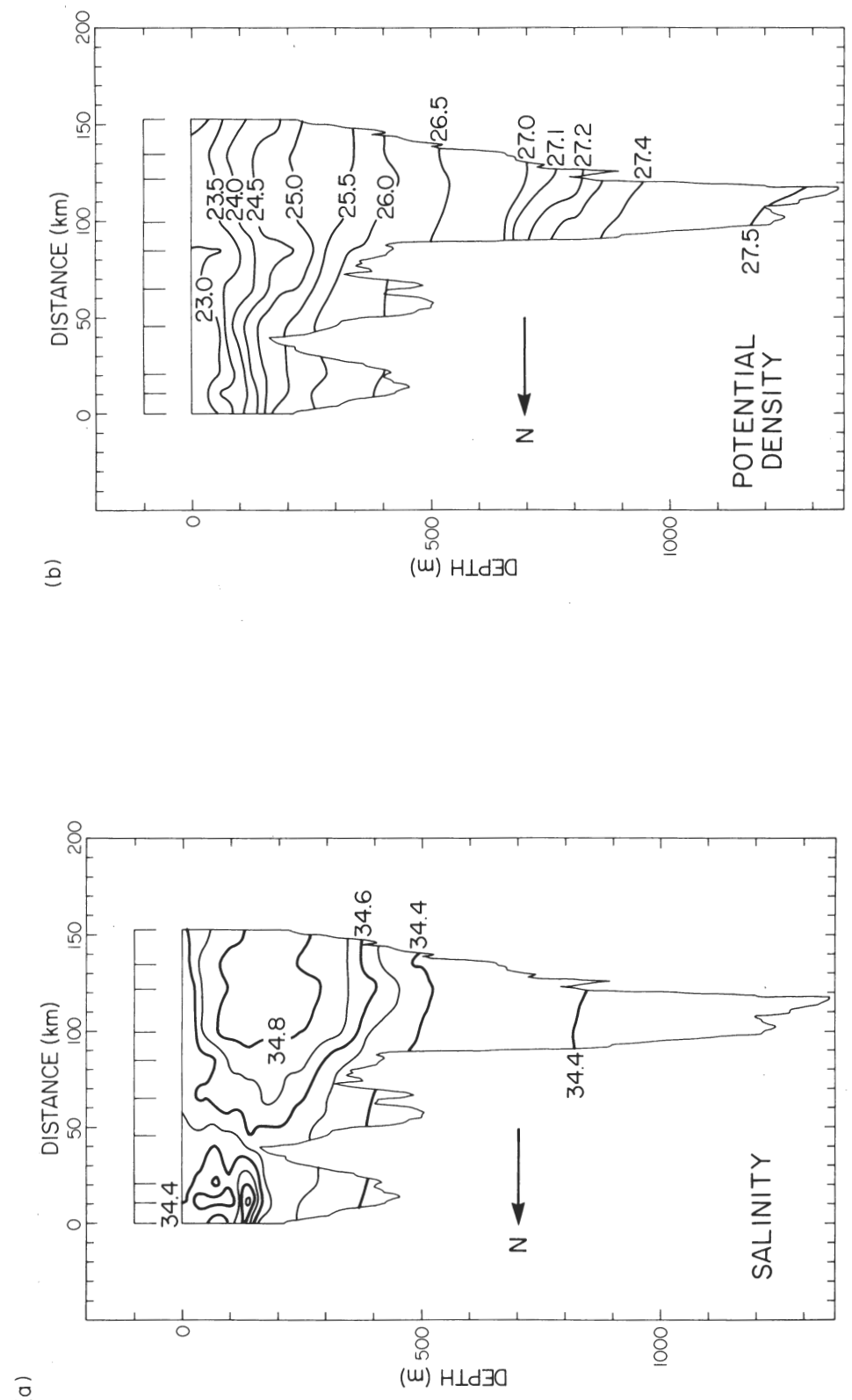

Fig. 3. Properties on the north section. Station locations are indicated above the section. 0 km is close to Kyusyu; 153 km is on the southwest end of the section. (a) Salinity (‰). (b) σ_θ (kg m^{-3}).

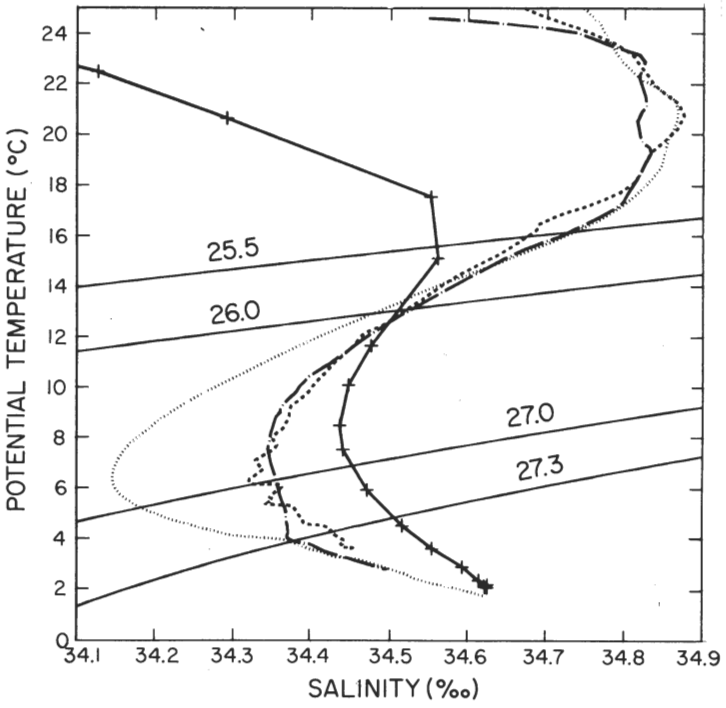

Fig. 4. Potential temperature–salinity relations. Four isopycnals are included. These correspond to boundaries between layers in the standard model. Dashed curve: deepest station on south section. Chain dashed curve: deepest station on north section. Dotted curve: a TPS24 station at 25°37′N, 127°25′E in the Philippine Basin. Solid curve marked with +s: a station taken by the *Hakuyo Maru* in the northern South China Sea at 18°26′N, 119°26′E on 19 July 1972.

water in the Philippine Basin, as previously noted by NITANI (1972) (Fig. 4). The North Equatorial Current ends at the western boundary of the Pacific in the area of the Philippines, where a part of the current turns northward and becomes the beginning of the Kuroshio. As this water moves northward past the strait between the northern Philippines and Taiwan, water at the density range of the North Pacific Intermediate Water mixes with more saline water from the South China Sea. Thus the intermediate waters of the beginning of the Kuroshio are more saline than those of the surrounding areas of the North Pacific. In a similar way, the water of the vertical salinity maximum also mixes with water from the South and East China Seas as it travels northward.

What is the densest water carried by the Kuroshio from the East China Sea, across the Tokara Straits, and through the north section? This question is critical for applying constraints to the inverse model in this study. Examination of historical hydrographic data in the vicinity of the 563 m sill (Fig. 1) showed no significant overflow of dense water from the Okinawa Trough into the Philippine Basin. Thus, an isopycnal at about 500–600 m on the inshore side of the north section, $\sigma_\theta = 27.0$, was chosen as the one most likely to be at the boundary between overflow and non-overflow. This choice is confirmed by TAKEMATSU *et al.* (1986), who found a boundary between the eastward-flowing Kuroshio and water flowing southwest along local isobaths at about 600 m.

A change in water properties occurs as the Nansei–Syoto Ridge is crossed from the Philippine Basin to the East China Sea (Fig. 5). The fact that the water properties are different means that only the water close to the ridge has a significant Philippine Basin component.

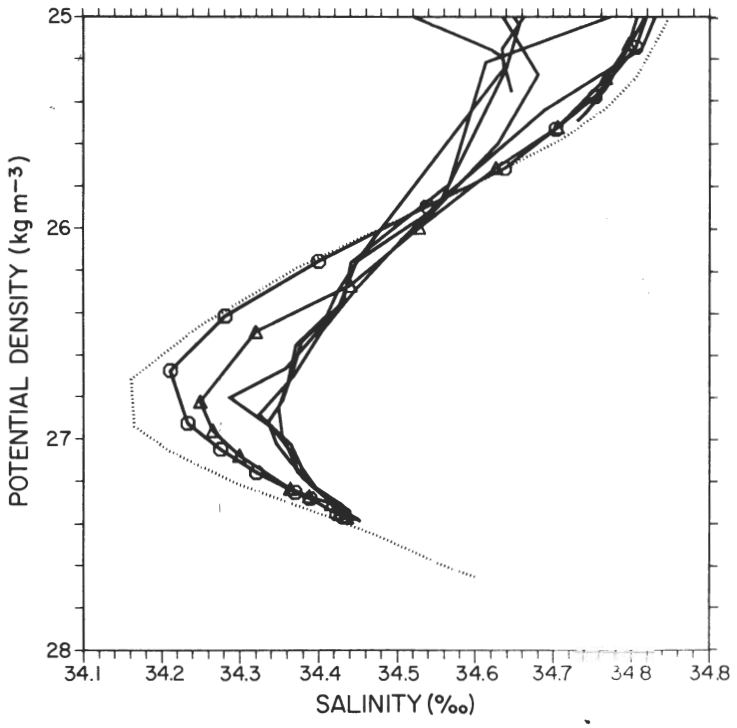

Fig. 5. Potential density (kg m^{-3}) vs salinity (‰). Dotted curve: a station at 25°37′N, 127°25′E in the Philippine Basin. Curve marked with circles: a station at 218 km in the south section. Curve marked with triangles: a station at 194 km in the south section. The other curves are stations at positions less than 194 km on the south section.

Geostrophic calculations

It is important at the beginning to estimate the uncertainties in the calculation of transport which are due to errors in the data alone. These sources of error include failure of the sampling scheme to adequately resolve variations in bottom topography and instrumental errors in measuring temperature, salinity and ship position.

When station spacing does not resolve the bottom topography adequately, large errors can occur in the shear extrapolated below the depth of the shallower station. Both sections include places where the bottom depth changes by more than 500 m between stations in areas of strong and highly variable shear (Figs 2 and 3). As is explained in ROEMMICH and MCCALLISTER (1989), objective mapping is the optimal method of extrapolating isopycnals into the bottom since it takes into account both the vertical and horizontal covariance of the data. Other methods, such as ignoring the flow below the deepest common depth of two station pairs, may be biased and certainly cannot take into account the horizontal covariance of the data. Data from the north section were objectively mapped; using a bottom level-of-no-motion and varying covariance functions, a spread in transport of ± 1 Sv was found with a mean transport of 18 Sv. The objective mapping procedure chosen was one that both agreed with the data and had no unexpected density or temperature inversions.

Other algorithms were tried for extrapolating shear into the bottom. The transport was computed using the smoothed 10 db data and assuming the bottom was at the shallowest depth of two stations of a pair. The north section transport, referred to the bottom, was

14 Sv. Another extrapolation method was to assume that the slope of the isopycnals was constant below the bottom of the shallower station. North section transport calculated by this method was an unreasonably large 42 Sv. The large transport came mostly from the area below the station pair at 84 and 99 km. The shear was large there because the deepest isotherm measured at the station at 84 km had a relatively large slope and this slope was extended all the way to the bottom by the extrapolation method.

Errors in navigation and density measurement also could affect the computation of geostrophic velocity and hence transport. Instrumental error in measuring density was not found to cause significant errors in transport measurement. Navigation errors are potentially significant in calculation of shear. However, errors in navigation tend to be negatively correlated with each other. An underestimate of the distance between one station pair will be associated with an overestimate of the distance between the following pair, so the corresponding errors in transport will be reduced.

3. INVERSE TECHNIQUE

The inverse technique used in this investigation starts out assuming that mass is conserved in the channel defined by the two sections in total and in a number of discrete layers. In addition it assumes no mixing across isopycnals and that the velocity is completely geostrophic. These assumptions lead to the system of equations

$$A\mathbf{b} = -\mathbf{\Gamma}, \tag{1}$$

where A is an M × N matrix whose elements (a_{ij}) are the area between station pair j in a density range i; $\mathbf{b}$, the solution, is an unknown N-vector of reference velocities at each station pair; and $\mathbf{\Gamma}$ is an M-vector whose elements (γ_i) are the amount by which density layer i is out of mass balance given the initial reference level for the geostrophic computation. This notation is the same as that of WUNSCH (1978). The equations (1) are solved by a technique called singular value decomposition (SVD) (WUNSCH, 1978; LANCZOS, 1961). Often A is not full rank, i.e. the rank of A is less than the minimum of M and N. The rank of A is called the cut-off of the SVD solution and is denoted as k. The residuals are the imbalances in each layer for a given solution $\mathbf{b}$, and are calculated by multiplying the matrix A and vector $\mathbf{b}$. The residuals might not be the same as $\mathbf{\Gamma}$ if A is not full rank.

The choice of k is rather subjective and, in the present study, was found to strongly affect the transport computed by the model. Unfortunately, the best choice is not obvious. In a number of previous studies (e.g. JOYCE *et al.*, 1986), the SVD solution was accompanied by a plot of solution vs residual magnitude. The best choice of a cut-off point was at the 'knee' of this curve, where a small decrease in residual magnitude is accompanied by a large increase in solution magnitude. In the present system that curve has no such knee and is thus no guide in determining the cut-off. A different approach is followed here. The solution vector $\mathbf{b}$, the transport through both sections, and the transport imbalances found in each layer are plotted for different values of k. The optimal value of k is one where the solution is not too variable and the layer imbalances are not too large.

The problem posed in (1) can be modified by row and column weighting (LAWSON and HANSON, 1974). In row weighting one divides each equation of the system (1) by the standard deviation of its associated element of $\mathbf{\Gamma}$. This is done to give each of the equations of (1) approximately unit variance. The solution found by SVD only makes sense if the

component equations have nearly the same uncertainty. It was found in this study that reasonable variations in row weighting had little effect on the results. Column weighting reflects a belief that a subset of the elements of **b** should have a certain size.

Two additions need to be made to WUNSCH's (1978) method. First, since the solutions are not unique, one can be found that emphasizes some subset of solution elements over another. Each column of this matrix is associated with a particular station pair. It might be known that some subset of station pairs has corrections which are larger, in the mean, than other station pairs. Considering two hydrographic sections at either end of a channel, it might be believed that the reference level velocities in one section are larger than those in the other section, on average, by a factor of ψ. This prejudice is incorporated into the inversion by defining a matrix $Q^{1/2}$. Let it be the N × N diagonal matrix with the elements in the columns associated with the larger corrections being $1/\sqrt{\psi}$ and all of the other elements 1. Then a new vector $\tilde{\mathbf{b}}$ is defined where

$$\tilde{\mathbf{b}} = Q^{1/2} b.$$

$\tilde{A}$ is then defined as

$$\tilde{A} = AQ^{1/2}$$

and the system of equations

$$\tilde{A}\tilde{\mathbf{b}} = -\mathbf{\Gamma}$$

is solved by singular value decomposition.

Secondly, prior knowledge about some part of the solution **b** is easy to incorporate into the SVD solution. This information may have been obtained by direct velocity measurement such as an acoustic Doppler current profiler (ADCP). Suppose it is desired that **b** be as close as possible to some independent estimate $\hat{\mathbf{b}}$. The N × N identity matrix is appended to A so that the left-hand side of the system of equations becomes an (M + N) × N matrix, and $\hat{\mathbf{b}}$ is added to the end of $\mathbf{\Gamma}$ to make the right-hand side an M + N vector:

$$\begin{bmatrix} A \\ I_N \end{bmatrix} \mathbf{b} = \begin{bmatrix} -\mathbf{\Gamma} \\ \hat{\mathbf{b}} \end{bmatrix}. \tag{2}$$

The system is solved as before by SVD. Alternatively, the vector $\mathbf{\Gamma}$ can be recomputed using $\hat{\mathbf{b}}$ as a reference for the geostrophic computation, calling it $\mathbf{\Gamma}'$. The inverse problem then becomes

$$A\mathbf{b} = -\mathbf{\Gamma}'. \tag{3}$$

The vector **b** becomes the misfit of the solution to $\hat{\mathbf{b}}$.

Eight principal physical assumptions were used in the model and each one was written as an equation.

1. Total mass was conserved within the channel. All water flowing into the channel through one section flowed out somewhere else. Loss of mass ('leakage') from the two sections via the Tsushima Current and the Osumi branch of the Kuroshio was estimated based on YI (1966) and NITANI (1972).
2. Mass was conserved within the layer σ_θ = surface–25.5. All leakage in assumption 1 was assigned to this layer. The 25.5 isopycnal was chosen because it is found at

approximately the depth of the Tsushima and Osumi Straits sills on the inshore side of each section.

3. Mass was conserved in the layer $\sigma_\theta = 25.5$–26.0.
4. Mass was conserved in the layer $\sigma_\theta = 26.0$–27.0.
5. All water flowing into the channel in the *south* section in the density range $\sigma_\theta = 27.0$–27.3 was assumed to flow out through that section.
6. All water flowing into the channel in the *south* section in the density range $\sigma_\theta = 27.3$–bottom was assumed to flow out through that section.
7. All water flowing into the channel in the *north* section in the density range $\sigma_\theta = 27.0$–27.3 was assumed to flow out through that section.
8. All water flowing into the channel in the *north* section in the density range $\sigma_\theta = 27.3$–bottom was assumed to flow out through that section.

Assumptions 5–8 express the fact that no water denser than $\sigma_\theta = 27.0$ is thought to flow over the sill at the Tokara Straits. The isopycnals bounding the density layers are displayed in Fig. 4.

How well should this system with a channel and two hydrographic sections conserve mass? The main places where mass can leak out of the system is through the Tsushima Current, the Osumi branch of the Kuroshio or across the Nansei–Syoto Ridge. YI (1966) estimated the average transport through the Tsushima Straits to be about 1.3 Sv, with seasonal fluctuations of about 1 Sv. ICHIKAWA (personal communication) has studied transport variations through the Osumi Straits and found that the transport never exceeds 3 Sv. NITANI (1972) esitmated the combined transport through the Tsushima and Osumi branches as a residual in the transport through a number of other straits. His average residual was 5 Sv, with temporal fluctuations between 0 and 10 Sv. There were no concurrent measurements of transport through these branches. The straits through which the Tsushima and Osumi branches flow are narrow and shallow, so it is difficult to believe that more than 10 Sv could be flowing through them. KONAGA *et al.* (1980) measured the flow across the Nansei–Syoto Ridge and found a small [O(1–2 Sv)] net transport outwards towards the Philippine Basin. On the other hand, ICHIKAWA (personal communication) has measured occasional, very large [O(25 Sv)] transports across the part of the ridge in question. The 'Prompt Report of Oceanic Conditions' (MARITIME SAFETY AGENCY, 1985) for the period when the sections were done shows no signs of strong surface or subsurface temperature fronts or currents going across the ridge between Okinawa and the north section, although the data available are incomplete. A guess of some positive leakage is probably better than zero so Nitani's average value of 5 Sv is used in all computations. The error in this value is about ±5 Sv. The Tsushima and Osumi Straits are at most 150 m deep so it is assumed that all of the leakage occurs in the layer between the surface and $\sigma_\theta = 25.5$, which is at about 150 m on the East China Sea side of both sections.

A problem related to leakage is that of temporary storage or depletion of mass in a layer. How much can a layer be reasonably out of mass balance? Suppose that at an instant the transport in one layer through the south section suddenly increased by 1 Sv. At an average velocity of 50 cm s^{-1} it would take 6–10 days for the extra water to propagate through the system and leave the north section. Since the sections were taken within 2 days of each other, the true solution of the absolute velocity could easily show 1 Sv more transport in one section than the other. If the entire imbalance were spread over the area between the sections the implied vertical velocity would be approximately 0.3×10^{-5} m s^{-1}, a reasonable amount to see for a short time. How much does transport through a given layer in one

section fluctuate on a time scale such that the fluctuation would not have had time to propagate through the system, i.e. less than 6–10 days? According to the results of NIILER and RICHARDSON (1973), the Florida Current fluctuates as much as 7–9 Sv over a time scale of 6–10 days. If this imbalance were divided into five layers, each layer would have a total imbalance of about 1.5 Sv at most. Since it is impossible to guess at the magnitude of any real temporary mass storage, it has been assumed that none occurs.

4. HYDROGRAPHIC DATA INVERSIONS

The inverse technique described in the previous section was applied to the channel defined by the two Kuroshio sections. Results are first discussed in terms of a standard model; the effects of varying assumptions are then described. The standard model consists of eight equations expressing conservation of mass in five layers, as outlined in the previous section. The first equation is the sum of the last seven, so that the rank of A is at most 7. The initial state for the standard model is zero velocity at the bottom. The inversion produces the bottom velocities which balance mass in the channel and are smallest in the r.m.s. sense.

Standard model

The results of the standard model (Fig. 6) show that most of the large corrections occur in the shallow parts of both sections, especially for larger values of k. These corrections allow the system to balance total mass without causing an imbalance in the second and third layers. Over the range of values of k the south section transport varies from 24 to 28 Sv and the north section transport varies from 18 to 23 Sv (Fig. 7). The best solution appears to be $k = 4$; both it and the $k = 5$ solution have residuals which are acceptably small, less than 1 Sv, and are not too variable. The $k = 4$ and $k = 5$ solutions differ principally in that the $k = 5$ solution has large corrections in the shallow parts of both sections, which are presumed to be unphysical. These large corrections add an extra 4 Sv to the transport. The $k = 4$ solution is chosen because it does not have these large corrections.

The signs of the residuals for both the $k = 4$ and $k = 5$ solutions vary with depth; in the top layer, the residual is negative, in the middle layer positive and in the bottom layer negative, so that averaged over the water column the total residual is small, less than 1 Sv. If the residuals had been of the same sign over a large fraction of the water column, then some difficulty with the way the problem was posed might have been suspected, possibly an unintended leakage.

The best solution of the model, $k = 4$, was examined in more detail. In the south section the geostrophic velocity field computed from this model (Fig. 8a) shows that the core of the Kuroshio is up against the shelf of the East China Sea. This section contains two counter-currents: one along the Nansei–Syoto Ridge extends from top to bottom. The other is underneath the strongest part of the Kuroshio on the shelf of the East China Sea. The strongest part of the second counter-current is at the depth of the salinity minimum of the North Pacific Intermediate Water. These counter-currents are the result of the imposition of no flow below sill depth, since counter-currents are necessary to bring deep water back through the south section to conserve mass.

In the north section the density field is more irregular and complicated than in the south section, and this is reflected in the velocity field (Fig. 8b). There are two or three different cores of the Kuroshio with counter-currents. This filamented structure is probably due to the presence of the Tokara Islands, just upstream of the Tokara Straits. NITANI (1972) noted that the striped character of the Kuroshio in the Tokara Straits disappears only 30–40 nmi downstream.

The counter-currents in the south section are the most interesting features of the model geostrophic velocities. The elements of the solution with the counter-currents between grid pairs 27 and 31 and pairs 37 and 39 (Fig. 6) confirm the existence of the counter-current along the Nansei–Syoto Ridge. The water at the two stations on the Nansei–Syoto Ridge resembles water found in the Philippine Basin. This anomalous water may flow through a gap in the Ryukyu Islands between Okinawa and Amamioshima in a direction opposite to the Kuroshio. This water is assumed to alter the properties found along the ridge but not to change the basic conservation assumptions in the model. As noted above, KONAGA *et al.* (1980) found a small [O(1–2 Sv)] net transport outwards, from the East China Sea into the Philippine Basin between Okinawa and Amamioshima. However, in the part of the gap just north of Okinawa there was a net transport in the other direction of about 1.5 Sv.

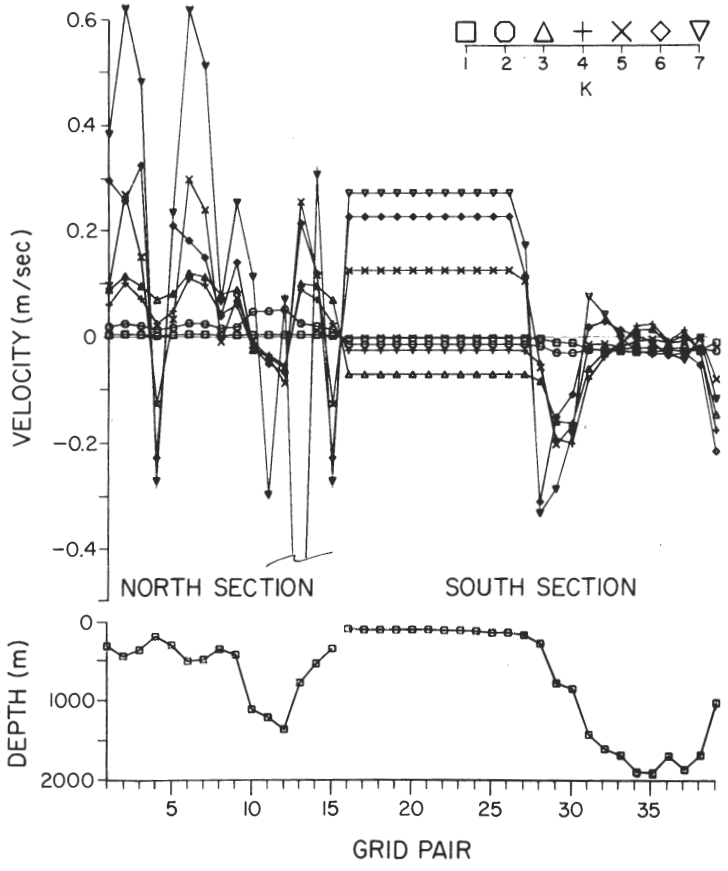

Fig. 6. Bottom velocities in m s^{-1} computed as a solution to the standard model as a function of grid pair. Grid pairs 1–15 are part of the north section and grid pairs 16–39 are part of the south section. Different symbols correspond to different ranks as indicated in the inset. At the bottom is the topography of the north and south sections in meters.

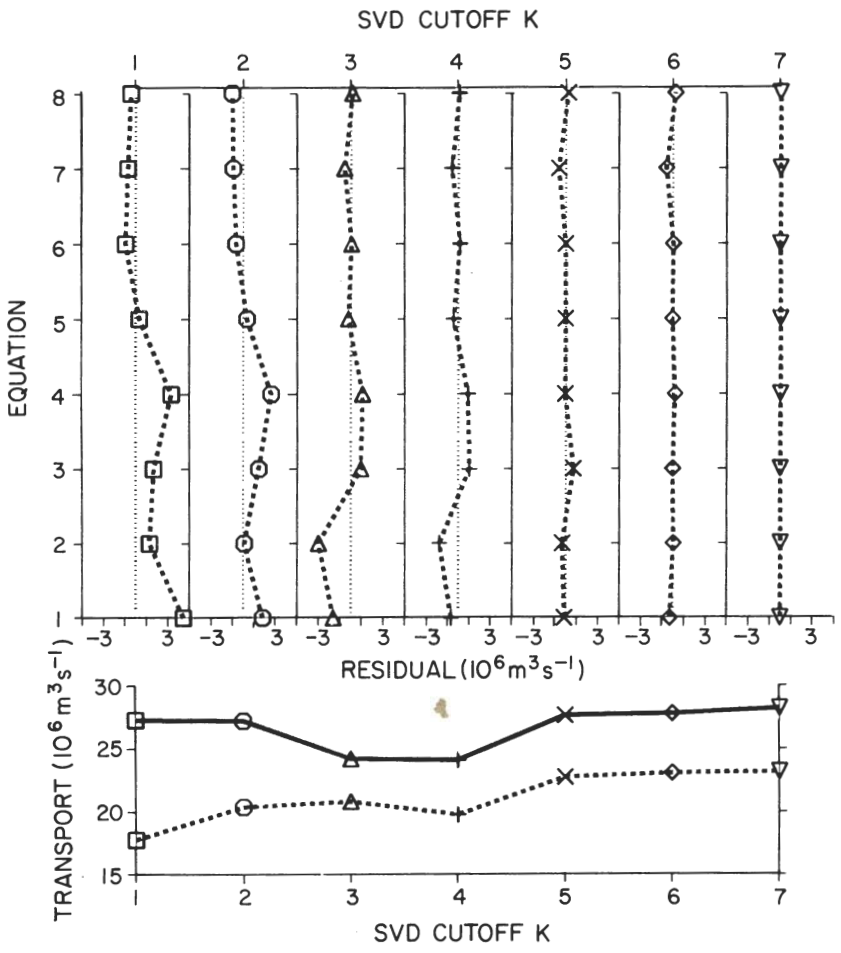

Fig. 7. Section transports and equation residuals for the standard model as a function of k, the assumed rank of the matrix A. Symbols correspond to those of Fig. 6. Transports and transport residuals are in Sv. Equations are described in Section 3. Solid line indicates south section transport. Dashed line indicates north section transport.

The Nansei–Syoto counter-current is a well-known feature of the East China Sea circulation (GUAN, 1988). PU and XU (1987) found a southward-flowing counter-current along the Nansei–Syoto Ridge using GEK data from 1972 to 1983 along the repeated Japanese section G-PN, just to the north of our south section. The counter-current was consistently present and had an average speed of about 20 cm s^{-1}. GUAN (1979) using GEK data from 1956 to 1975 along the G-PN section, found the counter-current in 51 of 54 crossings, with a maximum surface current velocity of 20–60 cm s^{-1}. KONAGA *et al.* (1980) also found counter-currents along the ridge and showed that the vertically integrated transport near the ridge was southward as well.

The second counter-current, on the slope of the shelf of the East China Sea, has no signature in the local water properties but resembles a current observed sometimes on the inshore side of the Florida Straits (BROOKS and NIILER, 1975). Perhaps it is part of a deep recirculation inside the Okinawa trough. PU and XU (1987) found a surface signature of this counter-current although it was not present as consistently as the current along the Nansei–Syoto Ridge. SUGIMOTO *et al.* (1988), reporting on current meter measurements on

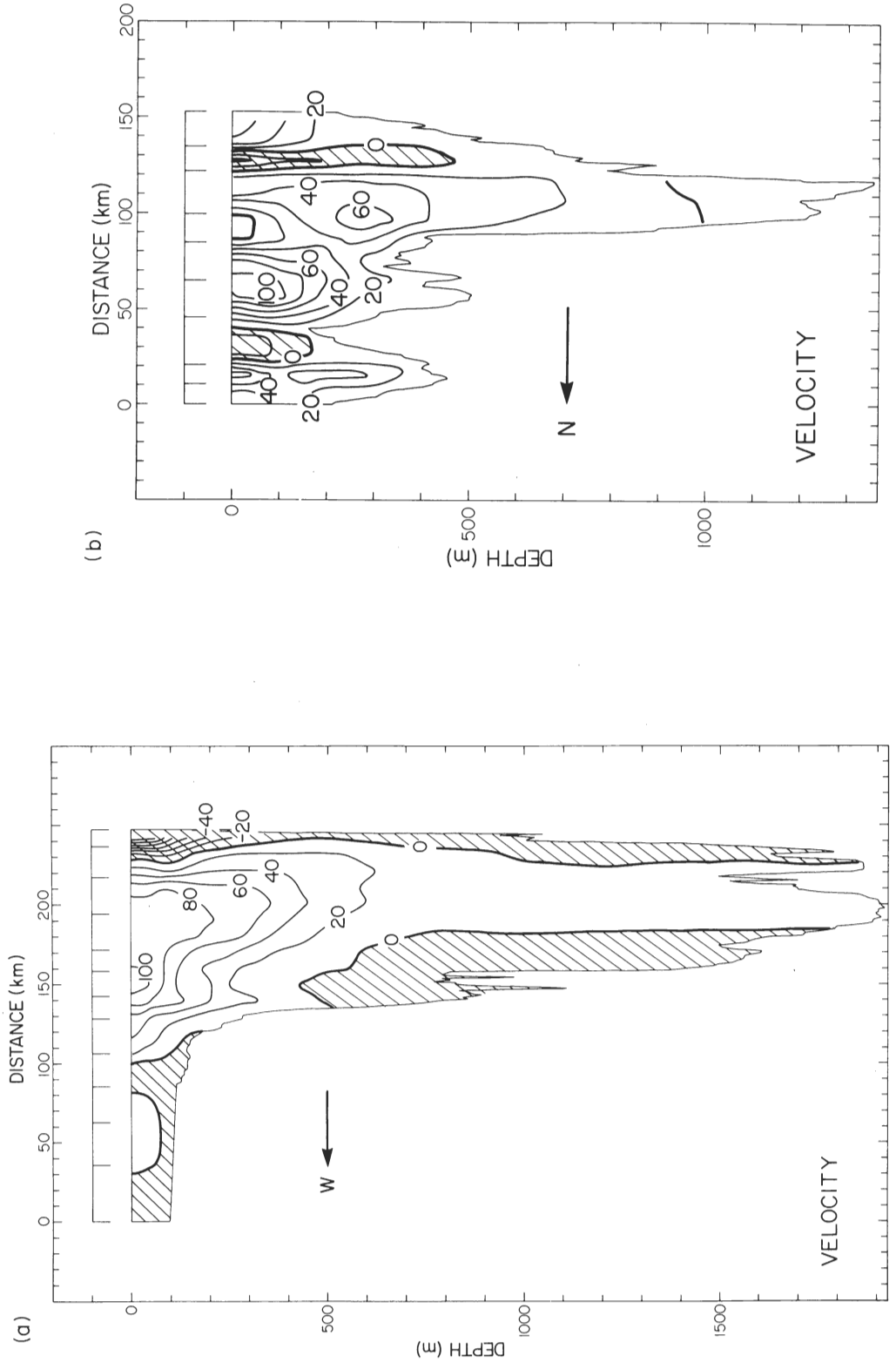

Fig. 8. Geostrophic velocity field in cm s^{-1} from best solution of the standard model. Positive velocities are in the direction of the Kuroshio. Negative velocities are hatched. (a) South section. (b) North section.

Table 1. *Transports in* Sv

	Standard model		Standard model with ADCP	
Density range	South section	North section	South section	North section
Total transport	24.1	19.8	26.6	21.9
Surface–25.5	16.5	13.3	18.6	14.7
25.5–26.0	3.1	2.1	3.8	2.4
26.0–27.0	4.8	3.9	4.3	4.2
27.0–27.3	−0.4	0.6	−0.1	0.9
27.3–bottom	0.1	0.0	0.0	−0.3

the slope of the East China Sea, also found the counter-current present a large fraction of the time.

The transport computed by the standard model is 24.1 Sv in the south section and 19.8 Sv in the north section (Table 1), within the range of those calculated by NITANI (1972) and KONAGA *et al.* (1980). The vertically integrated transport of the best estimate solution clearly shows the Nansei–Syoto Ridge counter-current in the south section and its associated strong anticylonic shear (Fig. 1). The transport of this counter-current is 3.4 Sv. The largest transports of the Kuroshio in the East China Sea are over the deep part of the Okinawa trough, although the strongest currents are along the continental shelf. The transport in the north section has a filamented, irregular structure consistent with NITANI's (1972) description.

Uncertainties

Many factors can be varied in the model. These include the initial state to which the model finds the closest solution, the number and configuration of the layers, the size of the leakage out of the top layer, and the relative expected sizes of the solution elements in the two sections. By varying these factors within reasonable bounds, it is possible to find a range of transports consistent with physically realistic assumptions.

Different initial reference level choices for the inverse were tried and transports resulting from them did not vary much (Fig. 9). In contrast, the transports computed as a function of reference level (with no inversion) illustrated a strong dependence on reference level. This result is probably a consequence of the topographic constraints applied to the model. Not allowing flow through in the deep layers severely restricted the amount of water that could be transported through the sections.

Different layer configurations were tried. The standard model has five layers, which was found to be the best compromise. Using more than five layers made little difference in the form of the solution. Using fewer than five layers inadequately resolved the vertical structure of the water column.

The north section transport was found to be much more sensitive than the south section to the size of the Tsushima–Osumi leakage (Fig. 10) Apparently the model was better able to force flow through the north section without disturbing the balance of deep water because the north section was generally shallower. This also means that the transport computed for the south section is more reliable than that for the north section as estimating this leakage is one of the main sources of error.

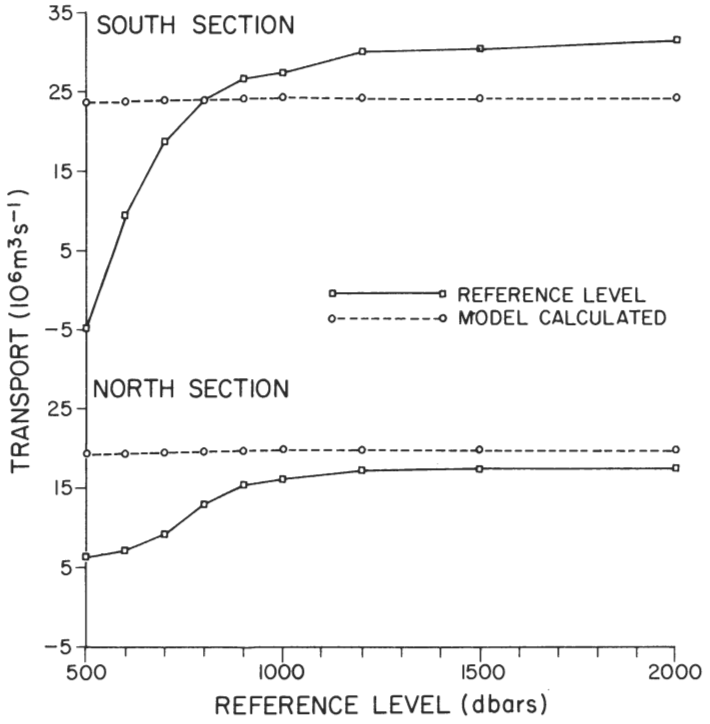

Fig. 9. Transport in Sv computed as a function of reference level through north and south sections. Solid curve: transport computed using pure reference level. Dashed curve: transport computed using reference level geostrophic velocities as input to the standard model.

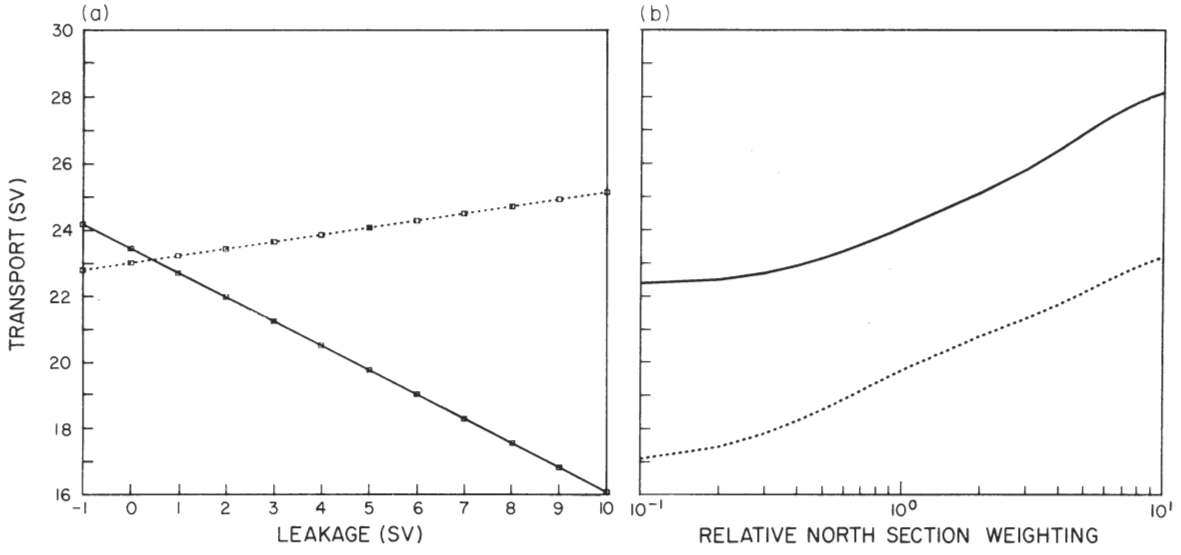

Fig. 10. (a) Transport in Sv computed by the standard model as a function of assumed Tsushima/Osumi leakage. Solid curve is the south section. Dashed curve is the north section. (b) The results of changing relative weighting of north and south sections. Solid curve is south section transport. Dashed curve is north section transport. See text for explanation.

Finally, if there is *a priori* knowledge that the bottom velocities in the north section differ on average from those in the south section, it is possible to incorporate this into the inversion by using an appropriate weighting as was described in Section 3. The standard model was run several times with different relative weightings on the solution elements in the north and south sections. When the relative importance of the north section (ψ in Section 3) was varied from 1 to 10, the transport computed by the standard model changed by 4 Sv (Fig. 10b). There are no direct velocity measurements in the area of the south section to determine what this weighting should be. The range of 1–10 is reasonable since it is plausible that the bottom velocities are larger in the north section, but it seems unlikely that they are more than an order of magnitude larger. This introduces an extra 4 Sv of uncertainty into the calculation of transport. It will continue to be assumed that the weighting is 1, but it should be kept in mind that a change in this number could mean a change in the computed transport.

The main sources of uncertainty in the model (Table 2) are the uncertainty in determining the cut-off of the SVD solution, the error in extrapolating isopycnals into the bottom in the objective mapping, the uncertainty in weighting different elements of the solution, and the transport imbalance or leakage imposed on the model. The sum of all of the errors except the cut-off error, assuming they are uncorrelated, is ±3.3 Sv in the south section and ±5.1 Sv in the north section.

ROEMMICH and MCCALLISTER (1989) computed a transport of 30.7 Sv through the south section. They combined the south section with the continuation of TPS24 along 24°N and a section along 137°E as part of an inversion of the entire North Pacific. They did not put explicit error bars on their estimates but their two alternative models had even larger transports. Why are our estimates different? There are several possible explanations. Perhaps the leakage out of the channel through the Tsushima and Osumi currents is larger than the previously estimated 5 Sv, although changing this parameter would not change the south section transport much. Secondly, our model minimizes bottom velocities or departures from a reference level, as does that of Roemmich and McCallister, but our model uses data from the north section, where theirs does not. In the north section the Kuroshio flows over shallow topography, and this initial guess may not be a good one. A larger emphasis in the model on solution elements in the north section leads to a higher north section transport and thus a higher south section transport. Thirdly, the north section is just downstream from the Tokara Islands and therefore the velocity structure there is more time dependent. Perhaps there is a storage of mass associated with the flow through the Tokara Islands. Lastly, Roemmich and McCallister used a 1981 section along 137°E in their mass conservation model. Perhaps the Kuroshio transport in 1981 across

Table 2. Sources in the standard model

Error source	Approximate magnitude in Sv
Cut-off choice	+4
Objective mapping and non-resolution of topography	1
Column weighting	3
Leakage/storage, south section	1
Leakage/storage, north section	4

137°E was larger in 1981 than in 1985, requiring a larger transport through the East China Sea to balance mass. As Roemmich and McCallister point out, these differences can only be resolved by time-series measurements of transport in the East China Sea.

5. ACOUSTIC DOPPLER CURRENT PROFILER DATA

The solutions obtained in the previous section were compared and combined with a set of ADCP data measured simultaneously. Joyce *et al.* (1986) successfully combined ADCP and hydrographic data in an inversion of Gulf Stream velocities. They used two sections across the Gulf Stream in a system of equations similar to (2), with the addition of a set of unknown cross-isopycnal velocities. Their sections were much deeper than those used here, going as deep as 4500 m. They also had no shallow sill between sections and thus no topographic constraint in their model. They found that the combination of ADCP and hydrographic data gave better results than using either set of data in isolation.

Data

Church and Joyce (1990) reported on the ADCP measurements made on TPS24. The ADCP data here are of poorer quality, especially in the north section, than in Joyce *et al.* (1986) because the connection between the ship's satellite navigation system and the ADCP instrument failed during TPS24. Thus only LORAN navigation was available for the Kuroshio sections which, unfortunately, were poorly situated for accurate LORAN navigation.

According to Kosro (1985), one of the main errors in translating ADCP velocities to velocities in geographical coordinates is the possible misalignment between the ship's compass and the fore direction of the ship. Church and Joyce (1990) computed this relative misalignment error for TPS24 and found it to be zero to within ±0.3°. Bryden *et al.* (1991) computed a misalignment error of 0.16° in the same ADCP data, based on mass conservation across 24°N which yields a northward velocity of 1.43 cm s^{-1}. Since both sections across the Kuroshio were crossed in the same orientation relative to the direction of the current and with approximately the same ship's speed, the misalignment error has a relatively small effect on mass conservation. In addition to bias error there are other random errors, including those associated with navigation problems. Bryden *et al.* (1991) used the ADCP data as a geostrophic reference only where an error tolerance of 13 cm s^{-1} was acceptable. This seemed reasonable considering the observed spread of across-ship-track velocities in the north and south sections.

Five minute average absolute velocities and across-ship-track averages between hydrographic stations (Fig. 11) were computed by Church (personal communication). South section abolute velocities are at 70 m and north section velocities are at 100 m. These depths were the best compromise between being away from the surface mixed layer and the bottom. For computational purposes the across-ship-track velocity profiles were interpolated to the objectively mapped grid points by cubic spline interpolation.

The ACDP measurements on the south section clearly show the Kuroshio and confirm the presence of a strong counter-current adjacent to the Nansei–Syoto Ridge. The currents in the vicinity of the ridge are complicated, varying strongly in direction and magnitude in a short distance. The across-ship-track currents are weak and opposite in direction to the Kuroshio in the shallow part of the south section. In the model of the previous section, the

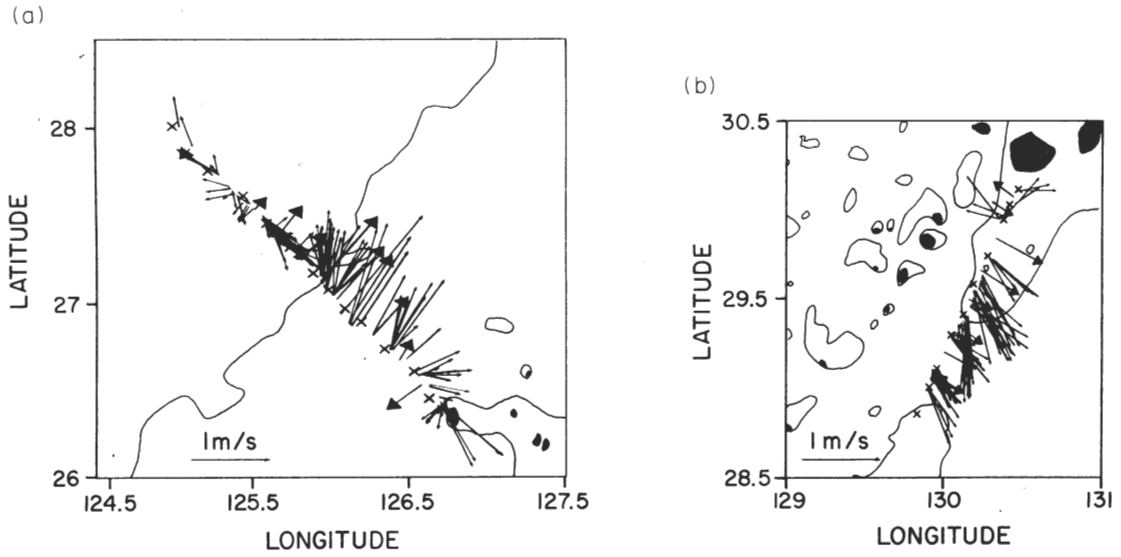

Fig. 11. Vectors with small heads: acoustic Doppler current profiler (ACDP) measurements of absolute velocity. Vectors with large heads: average across-ship-track ADCP velocities computed by Church. (a) South section, 70 m velocity. (b) North section, 100 m velocity.

difference between the $k = 4$ and $k = 5$ solutions was the presence of strong currents in the direction of the Kuroshio in the shallow part of the south section for $k = 5$. The ADCP data show no such strong currents and support the selection of $k = 4$ over $k = 5$. The counter-current found on the slope of the East China Sea by the standard model did not extend up as far as 70 m and thus would not be visible as a counter-current in the ADCP data.

Using ADCP data as the reference velocity without imposition of mass conservation resulted in unrealistically large mass imbalances in the surface layers (Table 3). Imbalances occur in the surface and mid-depth layers, the biggest being 3.1 Sv in the $\sigma_\theta = 26.0$–27.0 layer. On the other hand, the mass imbalances given by the ADCP reference are smaller than those given by the bottom reference level sometimes by as much

Table 3. *Mass imbalances in* Sv

Equation	Density range	Bottom reference	ADCP reference	Standard model	Standard model with ADCP
1	Total transport	8.9	4.8	−0.7	−0.3
2	Surface–25.5	2.2	1.1	−1.8	−1.1
3	25.5–26.0	1.9	2.1	1.0	1.4
4	26.0–27.0	4.2	3.1	0.9	0.1
5	27.0–27.3, south section	1.2	1.0	0.4	−0.1
6	27.3–bottom, south section	0.5	−1.3	0.1	0.0
7	27.0–27.3, north section	−0.7	1.1	−0.6	−1.0
8	27.3–bottom, north section	−0.4	−0.1	0.0	0.3

as 50%. Thus using ADCP data to define a reference level will not necessarily give a correct measurement of transport and its distribution with depth, but it may be better than use of an arbitrary level-of-no-motion.

Inverse calculations

ADCP and hydrographic data can be combined in inverse models in two basic ways, as described in Section 3. The ADCP can be used as an initial reference for the geostrophic velocities as is done in equation (3), or it can be used as a separate set of constraints as in equation (2). It was found in this study that the first method was preferable because of the potential problem of oversensitivity to weighting in the second method.

The ADCP data were first used to define an initial reference level; the residuals $\mathbf{\Gamma}'$ were calculated from the resulting geostrophic velocities based on the density field alone. An inversion was done using equations (3) and the same weighting, cut-off and layer configuration as in the model of the previous section. The transport computed was 26.6 Sv in the south section and 21.9 Sv in the north section (Table 1). The solutions, **b**, are very similar in structure to those obtained using an inverse with an initial reference level of zero velocity at the bottom. Both inverse solutions conserve mass. The actual velocities look somewhat different (Fig. 12), their different shapes being determined by the initial states from which they have minimum deviation. The r.m.s. size of **b** is less than 10 cm s^{-1}, within the error of the ADCP as described in Bryden *et al.* (1991). Because the initial imbalances in the layers were generally smaller for the ADCP reference than the bottom reference

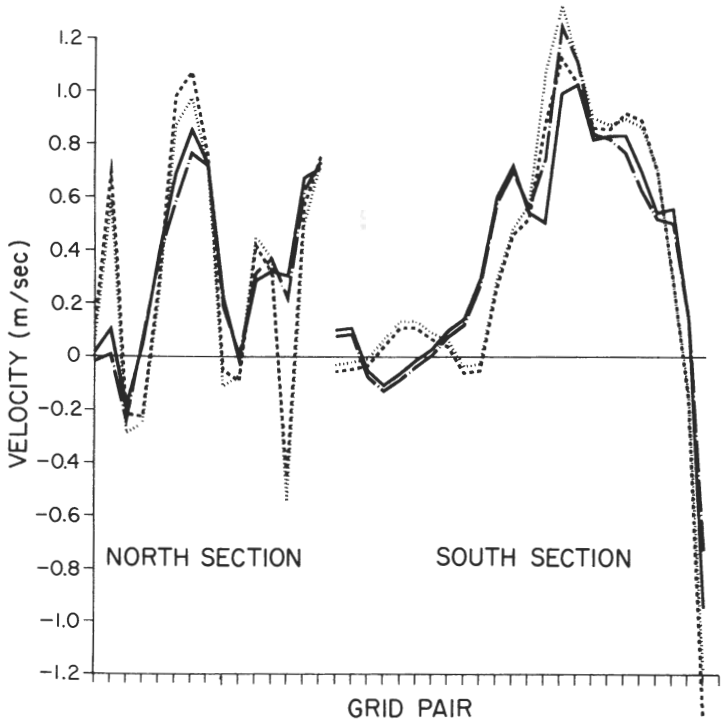

Fig. 12. Surface velocities from four different sources. Dotted curve: using zero velocity at the bottom as reference. Dashed curve: results of inverse model using bottom as initial reference. Chain dashed curve: using ADCP as reference. Solid curve: results of inverse model using ADCP as initial reference.

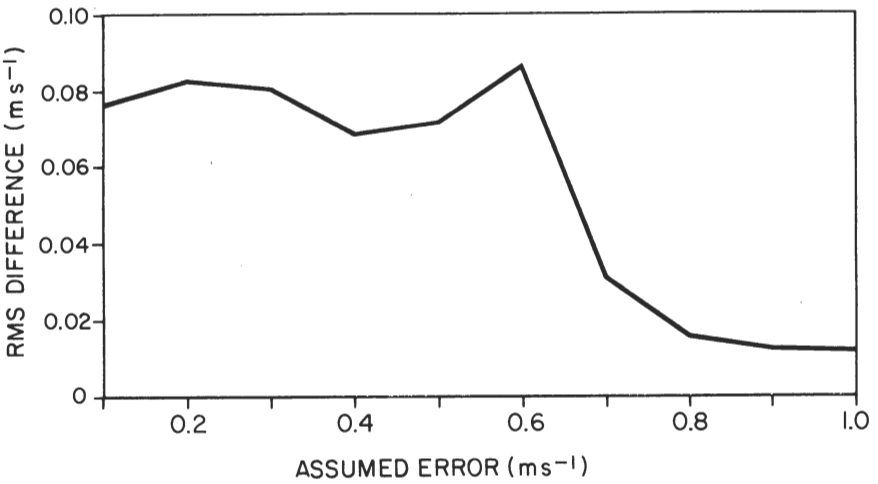

Fig. 13. Distance between a given model solution in r.m.s. m s^{-1} and the solution given by the standard model as a function of ADCP weighting or assumed error.

(Table 3), we consider the transports computed here to be more accurate than those of the previous section, although the two estimates differ by less than the calculated error of 3.3 and 5.1 Sv.

Using the second method of combining ADCP and hydrographic data, equations (2) were solved many times using different relative row weightings for the ADCP equations while holding the mass conservation weighting constant (Fig. 13). When the ADCP data are weighted heavily, i.e. given a small error, the solution is further away from the mass conservation solution as expected and vice versa. There is a sharp break at 0.6 m s^{-1} error. This is a transition from the inverse with bottom reference (the dashed curve) to the inverse with ADCP reference (the solid curve) solutions in Fig. 12. It may seem that 0.6 m s^{-1} is a large amount of error for ADCP velocities, but the weightings used for the mass conservation equations were only order of magnitude estimates and may be much too large. When mass conservation alone is used, the relative order of the weighting and not its size is important in the solution. Where information different from mass conservation is used, the relative weighting of ADCP and hydrographic data are crucial to the character of the solution. For this reason it was difficult to compare the results of this method of incorporating ADCP data with the results of the standard model in Section 4.

The two extremes in Fig. 13 are not significantly different, differing by only about 7–8 cm s^{-1} r.m.s. This is within the tolerance used by BRYDEN *et al.* (1991). The only place where the two solutions appeared to differ significantly was on the south section, close to the Nansei–Syoto Ridge, where the ADCP velocities were smaller than the velocities given by the inverse. The ADCP data show a smaller counter-current along the Ridge than the inverse solution. It would be hard to believe that the ADCP data are more accurate there, given the variations in magnitude and direction.

ADCP measurements can be used in inversions, but one must be careful of oversensitivity to weighting and also have a good idea where the ADCP data are reliable. In the present study, the ADCP data used as a reference for geostrophic calculations gave a better estimate of the absolute velocity than a reference level at the bottom. Incorporating the ADCP data as an initial state in the inversion was preferable to using the ADCP data as a set of separate constraints.

Acknowledgements—The Ocean Sciences Division of the National Science Foundation supported this work under grants OCE84-16211 and OCE87-40379. The TPS24 data were collected under NSF grant OCE83-17389. Computations were carried out on the Cray-XMP computer at the San Diego Supercomputer Center. J. Church and T. Joyce kindly furnished the ADCP data. We thank M. Tsuchiya, H. Ichikawa and an anonymous reviewer for their careful reading of the manuscript and their thoughtful comments. The TPS24 hydrographic data were supplied by D. Roemmich who provided the initial inspiration for this work and contributed to it in many important ways.

REFERENCES

Brooks I. H. and P. P. Niiler (1975) The Florida Current at Key West: Summer 1972. *Journal of Marine Research*, **33**, 83–92.

Bryden H. L., D. H. Roemmich and J. A. Church (1991) Ocean heat transport across 24°N in the Pacific. *Deep-Sea Research*, **38**, 297–324.

Church J. and T. Joyce (1991) Transpacific acoustic Doppler current profiling section across 24°N. *Deep-Sea Research*, in preparation.

Guan B. (1979) Some results from the study of the variations of the Kuroshio in the East China Sea. *Oceanologica et Limnologica Sinica*, **10**, 297–306 (in Chinese).

Guan B. (1983) Analysis of the variations of volume transports of the Kuroshio in the East China Sea. *Chinese Journal of Oceanology and Limnology*, **1**, 156–165.

Guan B. (1988) Major features and variability of the Kuroshio in the East China Sea. *Chinese Journal of Oceanology and Limnology*, **6**, 35–48.

Joyce T. M., C. Wunsch and S. D. Pierce (1986) Synoptic Gulf Stream velocity profiles through simultaneous inversion of hydrographic and acoustic Doppler data. *Journal of Geophysical Research*, **91**, 7573–7585.

Konaga S., K. Nishiyama and H. Ishizaki (1980) Geostrophic transport in the East China Sea and southeast of Yakushima Island—A case study. *Oceanographical Magazine*, **31**, 33–44.

Kosro P. (1985) Shipboard Acoustic Doppler Current Profiling during the Coastal Ocean Dynamics Experiment. PhD dissertation, Scripps Institution of Oceanography, University of California, San Diego, 119 pp.

Lanczos C. (1961) *Linear differential operators*, Van Nostrand, Reinhold, New York, 564 pp.

Lawson C. L. and R. J. Hanson (1974) *Solving least squares problems*, Prentice-Hall, Englewood Cliffs, New Jersey, 340 pp.

Maritime Safety Agency, Japan (1985) Prompt Report of Oceanic Conditions, no. 11, 15 May–4 June, 1985.

Niiler P. P. and W. S. Richardson (1973) Seasonal variability of the Florida Current. *Journal of Marine Research*, **31**, 144–167.

Nitani H. (1972) Beginning of the Kuroshio. In: *Kuroshio, physical aspects of the Japan Current*, H. Stommel and K. Yoshida, editors, University of Washington Press, Seattle, pp. 129–164.

Pu Y. and X. Xu (1987) The Kuroshio (on the PN section) in the East China Sea during 1972–1983. *Acta Oceanologica Sinica*, **6**, 37–45.

Roemmich D. (1979) The application of inverse methods to problems in ocean circulation. PhD dissertation, Woods Hole Oceanographic Institution, 193 pp.

Roemmich D. (1983) Optimal estimation of hydrographic station data and derived fields. *Journal of Physical Oceanography*, **13**, 1544–1549.

Roemmich D. and T. McCallister (1989) Large scale circulation of the North Pacific. *Progress in Oceanography*, **22**, 171–204.

Sugimoto T., S. Kimura and K. Miyaji (1988) Meander of the Kuroshio front and current variability in the East China Sea. *Journal of the Oceanographical Society of Japan*, **44**, 125–135.

Takematsu M., K. Kawatate, W. Koterayama, T. Suhara and H. Mitsuyasu (1986) Moored instrument observations in the Kuroshio south of Kyushu. *Journal of the Oceanographical Society of Japan*, **42**, 201–211.

Worthington L. V. and H. Kawai (1972) Comparison between deep sections across the Kuroshio and the Florida Current and the Gulf Stream. In: *Kuroshio, physical aspects of the Japan Current*, H. Stommel and K. Yoshida, editors, University of Washington Press, Seattle, pp. 371–385.

Wunsch C. (1978) The North Atlantic general circulation west of 50°W determined by inverse methods. *Reviews of Geophysics and Space Physics*, **16**, 583–620.

Yi S. (1966) Seasonal and secular variations of the water volume transport across the Korea Strait. *Journal of the Oceanographical Society of Korea*, **1**, 7–13.